PHOTONICS Research

Octave-spanning frequency comb generation based on a dual-mode microcavity laser

Ting Wang,[1,2] Ji-Liang Wu,[1,2] Xu-Cheng Zhang,[3] Yang Shi,[1,2] Yue-De Yang,[1,2] Jin-Long Xiao,[1,2] Da-Ming Zhang,[3] Guan-Shi Qin,[3] and Yong-Zhen Huang[1,2,*]

[1]State Key Laboratory of Integrated Optoelectronics, Institute of Semiconductors, Chinese Academy of Sciences, Beijing 100083, China
[2]Center of Materials Science and Optoelectronics Engineering, University of Chinese Academy of Sciences, Beijing 100049, China
[3]State Key Laboratory of Integrated Optoelectronics, College of Electronic Science and Engineering, Jilin University, Changchun 130012, China
*Corresponding author: yzhuang@semi.ac.cn

Received 2 May 2022; revised 15 July 2022; accepted 17 July 2022; posted 19 July 2022 (Doc. ID 462644); published 19 August 2022

Octave-spanning optical frequency comb (OFC) generation has achieved great breakthroughs and enabled significant applications in many fields, such as optical clocks and spectroscopy. Here, we demonstrate octave-spanning OFC generation with a repetition rate of tens of GHz via a four-wave mixing (FWM) effect seeded by a dual-mode microcavity laser for the first time, to our knowledge. A 120-m Brillouin nonlinear fiber loop is first utilized to generate wideband OFCs using the FWM effect. Subsequently, a time-domain optical pulse is shaped by appropriate optical filtering via fiber Bragg gratings. The high-repetition-rate pulse train is further boosted to 11 pJ through optimal optical amplification and dispersion compensation. Finally, an octave optical comb spanning from 1100 to 2200 nm is successfully realized through the self-phase modulation effect and dispersion wave generation in a commercial nonlinear optical fiber. Using dual-mode microcavity lasers with different mode intervals, we achieve frequency combs with octave bandwidths and repetition rates of 29–65 GHz, and demonstrate the dual-mode lasing microcavity laser as an ideal seeding light source for octave-spanning OFC generation.

https://doi.org/10.1364/PRJ.462644

1. INTRODUCTION

Optical frequency combs (OFCs) provide a time and frequency reference of optical waves and microwaves [1,2], which are powerful techniques in modern science and technology, such as optical clocks [3–5], spectroscopy [6–8], and distance measurements [9,10]. OFCs with repetition rates of 10 GHz and higher are required for applications of coherent optical communications [11,12], arbitrary waveform generation [13–15], and calibration of astronomical spectrometers [16]. In addition, high-repetition-rate OFCs have the advantage of accessible individual comb teeth, suitable for increasing the power per comb tooth to facilitate a high signal-to-noise ratio (SNR) [17,18]. Also, a tunable repetition rate makes OFCs more flexible in different applications. For example, flexible OFCs more easily meet the different channel spacings of massive parallel optical transmission [19]. Furthermore, multi radio-frequency (RF) signals with ultralow phase noise can be achieved via tunable OFCs [20]. Traditional mode-locked femtosecond lasers have a comb spacing of less than 1 GHz owing to a limited cavity length [21–23]. By using a tightly designed cavity, a 10-GHz OFC with a spectral range of 350 THz was realized in a Ti:sapphire laser [24]. However, long-term stable Kerr-lens mode-locking is a challenge for this design. Additionally, continuous-wave-driven optical microresonators are investigated widely to provide direct octave-spanning OFCs with a repetition rate up to THz [25–27]. Frequency combs based on cavities have a disadvantage that the repetition rate is not easily tunable. Subsequently, electro-optical modulation of a continuous wave is proposed to generate flexible OFCs with a tunable repetition rate of 10–30 GHz [28–32]. Recently, octave-spanning OFCs based on this scheme have been produced, and their phase coherence control and low-noise performance have been verified [33,34]. However, cascaded optical modulators are needed to enlarge the spectral range of OFCs due to the limited RF power of the microwave source, which increases system insertion loss and complexity.

Alternatively, the cascaded four-wave mixing (FWM) effect in highly nonlinear fibers (HNLFs) seeded by two continuous waves is another approach to generate high-repetition-rate OFCs with a flexible comb spacing and simple architecture [35–37]. To effectively broaden the comb spectrum, dispersion management techniques have been extensively studied and demonstrated for narrow pulses and wideband OFC generation [38–40]. By appropriately designed optical nonlinearity and dispersion, OFCs with a spectral range of more than 300 nm have been achieved [39]. Moreover, flat OFCs with

a power ripple of less than 6 dB in a 150-nm range were also demonstrated via this approach [40].

However, octave-spanning OFCs have not been realized via the FWM effect with dual pumps. This is attributed to two major challenges. First, stimulated Brillouin scattering (SBS) depletes the external pump light and limits the bandwidths of OFCs when the pump power reaches the threshold of the effect [41]. To solve this problem, a dual-wavelength Brillouin laser cavity was proposed to facilitate the Brillouin effect and enhance the FWM effect in the loop, resulting in high SNRs and narrow linewidths of comb lines [42]. Temporal cavity solitons and optical comb generation were investigated in a Brillouin laser cavity using the seeding sources of two external-cavity semiconductor lasers [43]. Furthermore, a frequency comb with a repetition rate of 76 GHz and bandwidth of 130 nm was realized using a Brillouin laser cavity with the seeding source of a dual-mode microcavity laser [44]. Second, an optical pulse at tens of GHz repetition rate has a limited pulse energy and is hard to give rise to a wideband spectrum. To obtain high peak power, an optical amplification and pulse shaping stage is crucial. Line-by-line pulse shaping is usually needed for spectral reshaping via a wave shaper, which increases cost and complexity [45].

Here, a flexible and simple approach is proposed to generate wideband OFCs by using a compact dual-mode seeding source. To the best of our knowledge, we demonstrate for the first time octave-spanning OFC generation via the FWM effect seeded by a dual-mode microcavity laser. This scheme has two advantages. First, a compact dual-mode semiconductor laser diode pumped SBS laser cavity gives rise to efficient and flexible OFC generation. The comb spacing is determined by the mode interval of the microcavity laser instead of two external discrete lasers in Refs. [35,36]. In addition, FWM efficiency is leveraged via a nonlinear fiber loop, as demonstrated in Refs. [42–44]. Second, a high-energy pulse is achieved through an optical amplifier and fiber Bragg grating (FBG) assisted pulse shaping. A complicated line-by-line shaping stage is avoided for system robustness and simplicity.

In this paper, octave-spanning OFCs with repetition rates of 29 to 65 GHz are achieved via the scheme. The nonlinear SBS loop is pumped by a dual-mode microcavity laser spaced at 50 GHz to generate a frequency comb with a bandwidth of 80 nm and more than 200 comb teeth. Wideband FBGs are adopted to suppress the pump light to narrow the optical pulse width from 6 to 1.6 ps. The amplified pulse is further narrowed to 379 fs via dispersion compensation after the erbium-doped fiber amplifier (EDFA) with a pulse peak power of 29.1 W. Finally, an octave-spanning OFC is realized with a spectral range from 1100 to 2200 nm by utilizing the self-phase modulation effect and dispersion wave generation in a commercial HNLF. Furthermore, octave-spanning frequency combs with repetition rates of 29, 50, and 65 GHz are generated using square microcavity lasers with different side lengths, which verifies the tunability of the proposed system. Beat frequencies of different spectral ranges of the OFC with narrow linewidths and low relative intensity noise (RIN) indicate a good coherence of the OFC. The proposed octave-spanning OFC has the potential to realize tunable mode spacing by using a tunable microcavity laser [46]. In addition, the obtained octave-spanning OFCs have a total power of more than 250 mW owing to the low loss in the commercial HNLF. The high optical power benefits the applications of optical sensing and optical coherence tomography.

2. EXPERIMENTAL SETUP

A schematic diagram of the octave-spanning OFC generator is shown in Fig. 1, which is composed of a seed source, a Brillouin fiber loop, and a nonlinear spectral broadening process. The output of the microcavity laser is coupled into a single-mode fiber (SMF) as a dual-wavelength light source. The coupled light is pre-amplified to 10 dBm by the low-power EDFA1, and passes through an optical bandpass filter (OBPF) to filter out unwanted side modes and amplified background noise. The filtered output light is amplified by the high-power EDFA2 and coupled into the Brillouin fiber loop as the pump light, where the pump light passes through a 120-m HNLF1 after entering an optical circulator (CIR). The zero-dispersion wavelength, dispersion slope, and nonlinear coefficient of the HNLF1 are 1535 nm, 0.017 ps/(nm^2 km), and 10.8 W^{-1} km^{-1}, respectively. When the pump power exceeds the Brillouin threshold, the SBS effect occurs and backward Stokes waves are generated. A polarization controller (PC) is used to adjust the polarization of the Stokes waves to achieve the largest Brillouin gain in the loop. The resulting Stokes waves cycle counterclockwise to lower the Brillouin threshold and improve FWM efficiency. As a result, a broadband Brillouin frequency comb with a high SNR is generated. It is worth noting that the repetition rate of the generated Brillouin OFC is equal to the mode interval of the dual-mode square microcavity laser. Then the Brillouin OFC is emitted from the 10% port of the 10-dB optical coupler (OC).

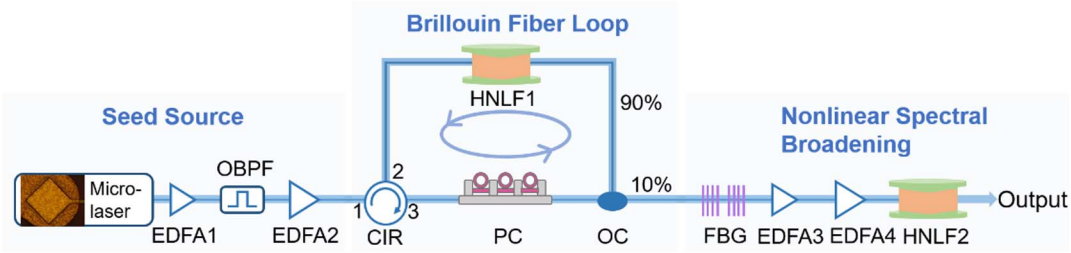

Fig. 1. Schematic diagram of the proposed octave-spanning OFC generator. EDFA, erbium-doped fiber amplifier; OBPF, optical bandpass filter; CIR, optical circulator; HNLF, highly nonlinear fiber; PC, polarization controller; OC, optical coupler; FBG, fiber Bragg grating.

An octave-spanning OFC with a high repetition rate is difficult to obtain owing to the low peak power of the optical pulse. Hence, the pulse width needs to be compressed for wideband OFC generation. The intensity of the Stokes light in the Brillouin frequency comb is very high, resulting in a sinusoidal waveform in the time domain. To reshape the optical pulse, wideband FBGs are used to suppress the intensity of the dual-mode Stokes light. The reflectivity and bandwidth of FBGs are designed as 99% and 2 nm, respectively. Then, the compressed pulse is amplified by cascaded EDFA3 and EDFA4 and further narrowed via fiber dispersion compensation. Finally, the high-energy femtosecond pulse undergoes self-phase modulation and dispersion wave effects through an 80-m HNLF2 to realize an octave-spanning OFC. The HNLF2 is composed of HNLFs with zero-dispersion wavelengths of 1520 and 1535 nm. Other parameters are the same as HNLF1. In the experiments, the frequency- and time-domain characteristics of OFCs are analyzed using an optical spectrum analyzer, a frequency-resolved optical gating, and an electrical spectrum analyzer equipped with a high-speed photodetector.

3. RESULTS

A. Lasing Characteristics of Dual-Mode Microcavity Laser

A square microcavity laser with a side length of 30 μm and output waveguide width of 2 μm is used as a seed source for octave-spanning OFC generation. The microcavity laser is manufactured using an AlGaInAs/InP epitaxial wafer with six pairs of compressively strained quantum wells as in Ref. [47]. The lasing characteristics of the microcavity laser fixed on a thermoelectric cooler maintained at 288 K are measured by coupling the laser output into a tapered SMF. The threshold current of the microcavity laser is 8 mA, and the maximum coupling power is 51 μW at 54 mA, as shown in Fig. 2(a). In addition, a series resistance of 13 Ω is obtained by linearly fitting the *V-I* curve around 46 mA. Stable dual-mode lasing around 1558 nm is achieved as shown in the lasing spectrum map in Fig. 2(b), which is measured using an optical spectrum analyzer with a resolution of 0.02 nm. Figure 2(c) shows the wavelength interval and intensity ratio versus the injection current. The wavelength interval of the dual-mode varies from 0.39 to 0.415 nm when the injection current increases from 44 to 56 mA. The detailed lasing spectra at 46 mA are shown in Fig. 2(d), with fundamental and first-order transverse mode wavelengths of 1557.813 and 1557.407 nm, respectively. The corresponding intensity ratio of the dual mode is less than 1 dB, ensuring an efficient non-degenerate FWM process.

B. Brillouin Comb Generation and Pulse Shaping

A proof-of-concept experiment is carried out based on the system setup in Fig. 1. As the optical power of the dual-mode microcavity laser is increased to 14 dBm, Brillouin Stokes light reaches its threshold in the SBS fiber cavity. The dual-wavelength Brillouin laser circulating in the loop acts as a new pump source to generate a broadband optical comb. It should be noted that the frequency spacing of the OFC is the same as the mode interval of the dual-mode microcavity laser, which is a multiple of the free spectral range (1.6 MHz) of the Brillouin fiber loop. When the output power of the microcavity laser is enhanced to 26.5 dBm, the spectral range of the Brillouin OFC extends to 80 nm, as shown in Fig. 3(a).

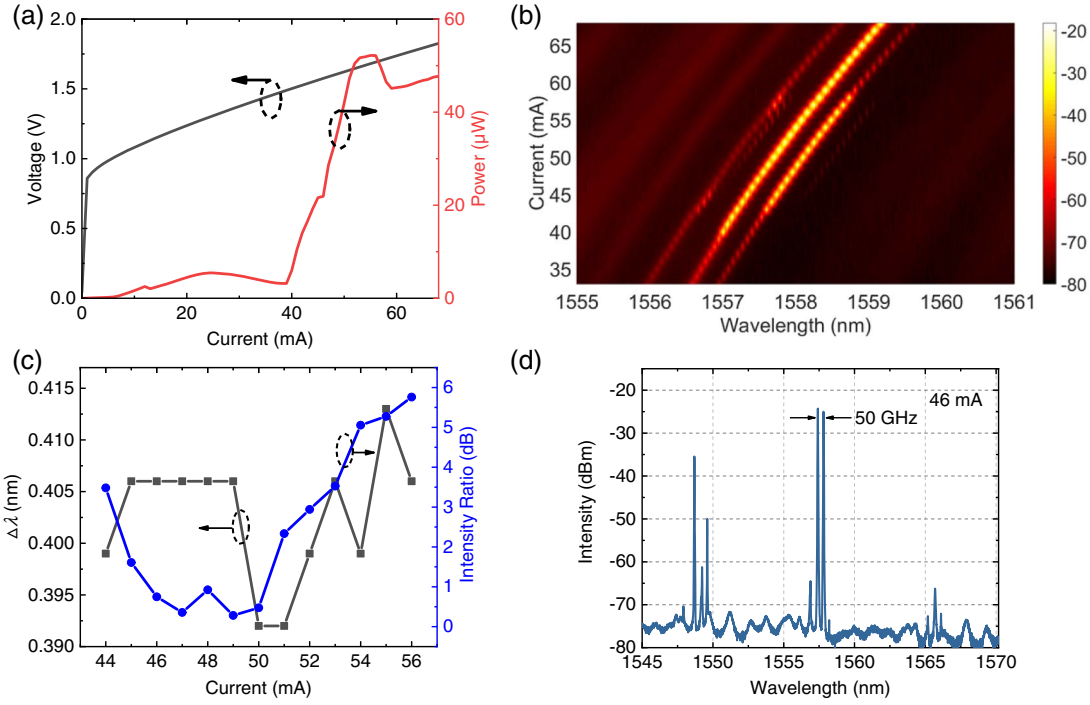

Fig. 2. (a) Output power and applied voltage versus injection current. (b) Lasing spectra map versus injection current. (c) Wavelength interval and intensity ratio of dual modes versus injection current. (d) Lasing spectrum at injection current of 46 mA.

Owing to the limited FWM parametric gain spectrum, the bandwidth of the optical comb is hardly increased by further improving the EDFA power. As a result, nonlinear spectral broadening is adopted for octave-spanning OFC generation, and thus a high-energy optical pulse is desired.

However, the time-domain pulse of the SBS optical comb has a relatively large duration, because the intensity ratio between the Brillouin laser and the newly generated frequency component is as large as 13 dB as shown in Fig. 3(a). A waveform in the time domain as shown in Fig. 3(b) is measured for the Brillouin optical comb using frequency-resolved optical gating. The measured autocorrelation trace is almost a sine wave with a period of 20 ps, corresponding to a comb spacing of 50 GHz. The pulse width is fitted to be 6 ps assuming a Gauss profile, and thus a pulse narrowing stage is necessary. An effective way to manipulate the optical pulse shape is line-by-line shaping via a wave shaper. However, this method brings about additional system insertion loss and complexity. To realize pulse narrowing via a simple approach, cascaded FBGs are used to suppress the Stokes light for spectral reshaping. The FBGs are designed to have 99% reflectivity and a wide stopband of 2 nm. As shown in Fig. 3(a), the Stokes waves are well suppressed after passing the two FBGs, and a flat-top spectrum is obtained. Furthermore, the measured autocorrelation curve of the suppressed optical pulse train is depicted in Fig. 3(b), which shows a significantly compressed pulse width of 1.6 ps.

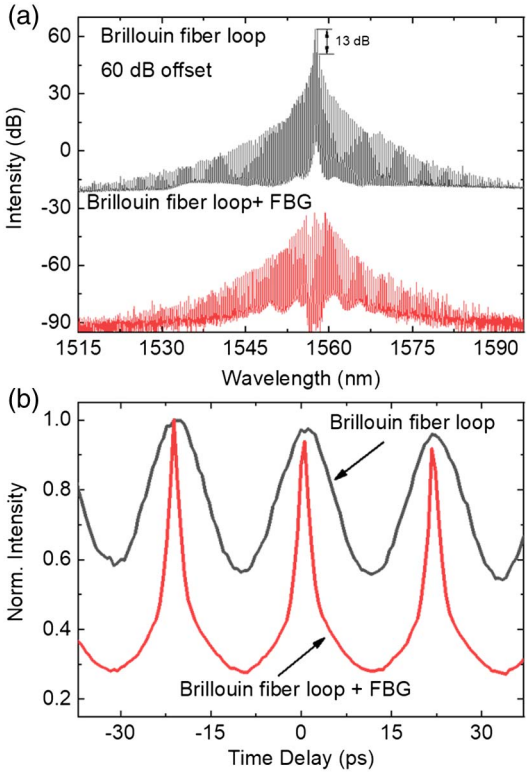

Fig. 3. (a) Output spectra of 50 GHz spaced Brillouin OFCs before and after optical spectral filtering of two FBGs. (b) Measured autocorrelation traces of the optical pulse train before and after optical filtering of two FBGs.

C. Octave-Spanning Optical Comb Generation

Subsequently, an optical amplification and dispersion compensation stage is managed to improve the optical pulse energy for further nonlinear spectrum broadening. The 1.6-ps optical pulse is pre-amplified by low-power EDFA3 and then amplified by high-power EDFA4 to obtain a high average power. Then, a piece of SMF with anomalous dispersion is applied for eliminating the chirp of the amplified pulse, thus obtaining high peak power. Moreover, accounting for the dispersion compensation connected with the nonlinear effect in EDFA4, the pulse shape is also investigated under different EDFA4 powers. Figure 4(a) shows the pulse width and pedestal-to-peak ratio versus EDFA4 power. The pedestal is defined as the part of the pulse that cannot be fitted by the Gaussian function. When the pump power is increased from 10 to 550 mW, the pulse width is gradually narrowed from 627 to 379 fs. With further increasing pump power, the pulse width is almost unchanged at around 370 fs. On the other hand, due to the amplified background noise in EDFA4, the pedestal intensity starts to increase when the pump power exceeds 100 mW. Therefore, EDFA4 power is set as 550 mW considering a narrow pulse width and low pedestal intensity. The gray dashed line in Fig. 4(b) shows the pulse emitted from the Brillouin fiber loop filtered by FBGs. In contrast, the pulse as the blue solid line is significantly narrowed owing to the combined effect of the dispersion in SMF and the nonlinear effect in EDFA4. A larger pedestal can be observed, which is caused by the amplified spontaneous emission noise and high-order dispersion in EDFA4. Hence, only the main pulse in the center of the autocorrelation trace is fitted instead of the low-power pedestal. The fitting pulse width is 379 fs, corresponding to a pulse peak power of 29.1 W and pulse energy of 11 pJ.

Furthermore, an 80-m HNLF2 is pumped to perform nonlinear spectral broadening. The evolution of the optical spectrum with EDFA4 power is shown in Fig. 4(c). Two optical spectrum analyzers are used to measure the octave-spanning OFC, with spectral ranges of 600–1700 and 1200–2400 nm. When the pump power increases to 550 mW, the spectral width reaches 1100 nm. The short-wave part spreads to around 1000 nm with the pump power increasing, while the long-wave part hardly changes. The specific broadening spectrum is depicted in Fig. 4(d) when the pump power is 550 mW. The results show that the broadband optical comb with a repetition rate of 50 GHz covers an octave, ranging from 1100 to 2200 nm. It is noted that pump light located in the anomalous dispersion region of HNLF can achieve broadband frequency combs and support soliton propagation [48]. The broadband dispersion of HNLF2 is depicted by the red line in Fig. 4(d). The zero-dispersion wavelengths of the HNLF are 1520 and 1535 nm, which are located on the blue side of the pump light. This meets the requirements for the generation of dispersive waves. Based on the phase matching equation, the dispersive waves will appear at $\omega = \omega_0 + 3|\beta_2|/\beta_3$ [49], where ω_0, β_2, and β_3 are the central angular frequency of the pump light, and second- and third-order dispersions at the pump light, respectively. The dispersion waves are calculated at wavelengths of 1410 and 1475 nm for HNLFs with zero-dispersion wavelengths of 1520 and 1535 nm, respectively, with $\beta_2 = -1.51$ and -0.68 ps^2/km and $\beta_3 = 0.036$

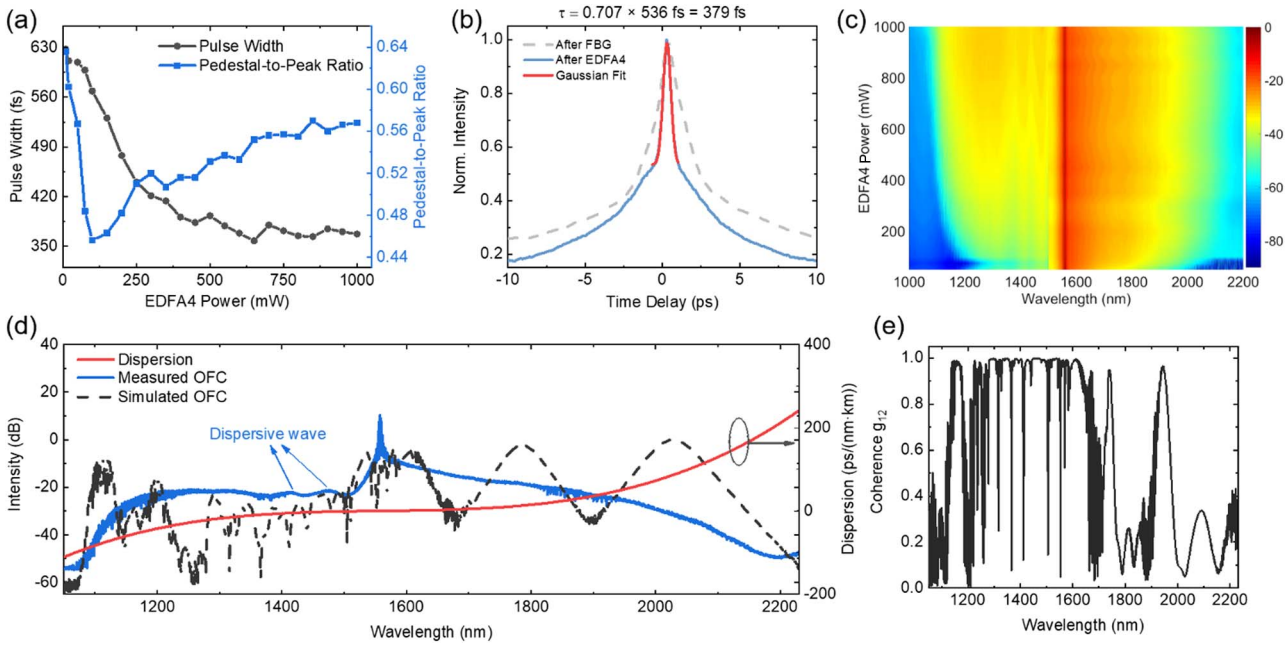

Fig. 4. (a) Pulse width and pedestal intensity versus EDFA4 power. (b) Measured autocorrelation traces of optical pulses when the pump power is 550 mW. (c) Evolution of the optical spectrum versus EDFA4 power. (d) Optical spectrum of the octave-spanning OFC when pump power is 550 mW. The red line represents the dispersion of HNLF2. The dashed black curve is the simulated octave-spanning OFC spectrum. (e) Degree of coherence of the simulated spectrum.

and 0.031 ps^3/km. The generated dispersive waves provide a spectral broadening in the normal dispersion region, as shown in Fig. 4(d), which is consistent with the calculated results.

The coherence of the OFC is also estimated using the nonlinear Schrödinger equation to model the spectral evolution in the optical fiber [50]. In the simulation, a Gaussian pulse with a pulse width of 250 fs and peak power of 90 W is used to pump an 80-m HNLF. Input pulse noise is considered using commonly adopted quantum noise models, and the coherence property of the resulting spectrum is calculated via $|g_{12}^{(1)}(\lambda)| = |\langle E_1^*(\lambda)E_2(\lambda)\rangle/[\langle|E_1(\lambda)|^2\rangle\langle|E_2(\lambda)|^2\rangle]^{1/2}|$ [51]. The nonlinear coefficient, and second- and third-order dispersion coefficients at the pump light of the HNLF are set as 14 $W^{-1}\,km^{-1}$, −1.1 ps^2/km, and 0.011 ps^3/km, respectively. It is slightly different from the dispersion values given before due to the comprehensive consideration of fibers with different dispersions. The simulated optical spectrum is shown as the dashed black curve in Fig. 4(d). The difference in spectral shape between the simulation and experiment comes from the pulse settings and dispersion parameters, since the actual pulse is not a standard Gaussian pulse. The coherence degree reveals that the OFC is partially coherent, as shown in Fig. 4(e). In the future, pulse shaping techniques can be optimized to further narrow the optical pulse from the SBS loop to improve the spectral coherence of the octave-spanning OFC generated in the HNLF.

The tunability of the repetition rate of the proposed OFC generator is also investigated. The generated optical combs with different repetition rates are realized using square microcavity lasers with different side lengths. Using the experimental setup in Fig. 1 and similar pump power as in Fig. 4(d), octave-spanning optical combs are obtained using three dual-mode lasing microcavity lasers with frequency intervals of 29, 50, and 65 GHz, and their spectral ranges are from 1100 to 2200 nm, as shown in Fig. 5(a). The corresponding fine spectra around the pump light are also depicted in Fig. 5(b).

Finally, the electrical spectral characteristics of the generated octave-spanning optical combs are investigated for an optical comb with a repetition rate of 29 GHz, which is limited by the bandwidth limitation of the electrical spectrum analyzer and photodetector. First, the optical comb is detected directly by a 50-GHz photodetector, and the obtained beat note is shown as the black curve in Fig. 6(a). The microwave spectrum contains a 29-GHz signal, indicating that the comb teeth are equally spaced. It is worth noting that the beat signal is composed of longitudinal modes with a 1.6-MHz interval, corresponding to the length of the Brillouin fiber loop. Figure 6(b) further shows the detailed electrical spectrum of the 29-GHz signal with a resolution bandwidth of 100 kHz and a range of 2 MHz. The linewidth of one of the longitudinal modes is 295 kHz by Lorentz fitting, which demonstrates the high coherence of the generated optical comb. The beat note linewidth of the corresponding dual-mode lasing microcavity laser is 35 MHz, which is about two orders larger than that in Fig. 6(b). On the other hand, the spectrum of the octave-spanning comb is not flat, and the frequency components near 1560 nm have higher energy. Therefore, an optical filter with a center wavelength of 1310 nm and bandwidth of 18 nm is used for further measurement. Then the filtered frequency comb is detected by the photodetector and depicted as the red curve in Fig. 6(a). There is only a 29-GHz microwave signal in the range of 44 GHz, which proves that the optical comb still maintains a frequency interval of 29 GHz near

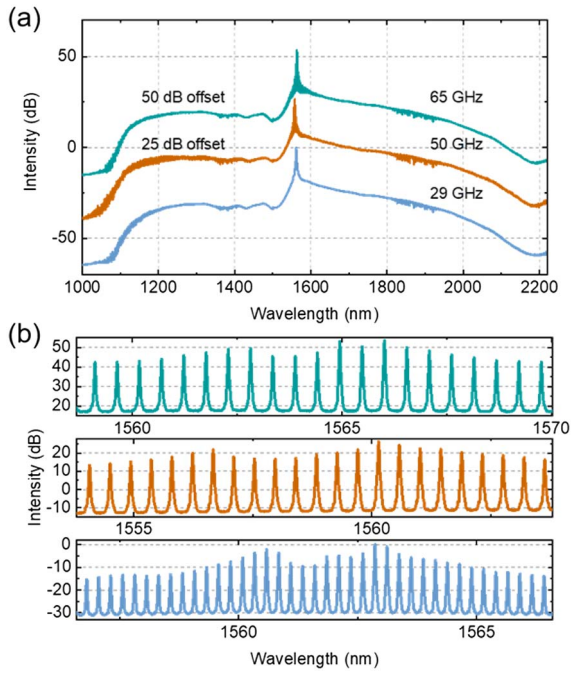

Fig. 5. (a) Octave-spanning OFC spectra and (b) corresponding fine spectra around the pump light, using square microcavity lasers with lasing mode frequency intervals of 29, 50, and 65 GHz.

1310 nm. Furthermore, the linewidth of 302 kHz is obtained in Fig. 6(c), which shows that the coherence is maintained at 1310 nm.

Next, the RIN of the octave-spanning OFC is measured. The electrical signal of the OFC obtained by a photodetector (PD) is divided into direct current and alternating current components through a bias-tee. The alternating current signal is amplified by a low-noise RF amplifier with a bandwidth of 0.1–40 GHz, which is considered as the total noise. The intrinsic RIN of the OFC can be obtained by subtracting the system thermal noise and photodetector shot noise from the total noise. Figure 6(d) shows the measured RIN, and the beat frequency between the multi-longitudinal modes of the Brillouin fiber loop results in a strong oscillation from −125 to −100 dBc/Hz at 100 MHz. The lower RIN of −140 dBc/Hz is observed around 3 GHz. Therefore, the above results indicate that the generated octave-spanning OFC has high coherence. In the future, the stabilization of OFC should be further improved by selecting a single longitudinal mode of the Brillouin fiber loop and the self-referencing technique.

4. CONCLUSION

In summary, we have proposed and demonstrated a high-repetition-rate octave-spanning OFC generator using a dual-mode microcavity laser. A microcavity laser with a dual-mode spacing of 50 GHz was used as a seed source to achieve 80-nm bandwidth in a nonlinear fiber loop, and the optical pulse was compressed to 1.6 ps via spectral reshaping using FBGs. Furthermore, the pulse after FBGs was not only amplified by EDFA, but also compressed to 379 fs owing to the nonlinear effect through optimizing the pump power. An octave-spanning frequency comb ranging from 1100 to 2200 nm was finally produced in an 80-m HNLF. In addition, to verify

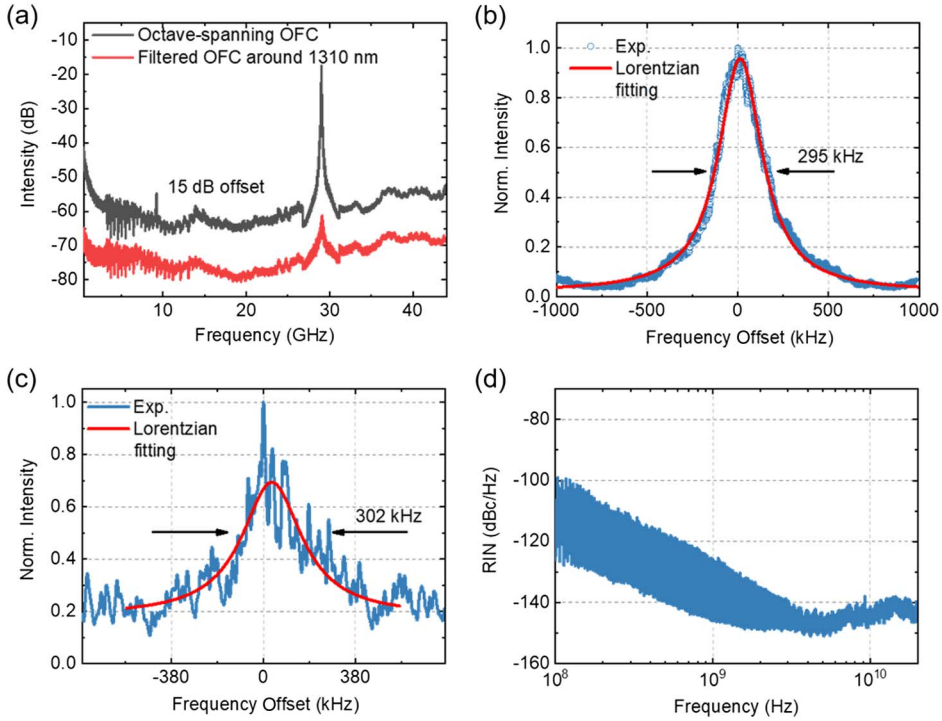

Fig. 6. (a) Electrical spectrum characteristic of the 29-GHz octave-spanning OFC and filtered OFC around 1310 nm. (b) Electrical spectrum within 2-MHz span of the octave-spanning OFC. (c) Electrical spectrum within 1.5-MHz span obtained from the filtered OFC around 1310 nm. (d) Relative intensity noise of the octave-spanning OFC.

the tunability of the repetition rate of the proposed system, octave-spanning optical combs with repetition rates of 29, 50, and 65 GHz were presented using different dual-mode lasing microcavity lasers. Finally, the beat notes and the RIN of the optical comb were measured to demonstrate a high coherence of the generated OFC. The proposed octave-spanning OFC shows good application potential in high-precision measurements due to its wide spectral range and simplicity.

Funding. National Natural Science Foundation of China (61527823, 61875188).

Disclosures. The authors declare no conflicts of interest.

Data Availability. Data underlying the results presented in this paper are not publicly available at this time but may be obtained from the authors upon reasonable request.

REFERENCES

1. D. J. Jones, S. A. Diddams, J. K. Ranka, A. Stentz, R. S. Windeler, J. L. Hall, and S. T. Cundiff, "Carrier-envelope phase control of femtosecond mode-locked lasers and direct optical frequency synthesis," Science **288**, 635–639 (2000).
2. S. A. Diddams, K. Vahala, and T. Udem, "Optical frequency combs: coherently uniting the electromagnetic spectrum," Science **369**, eaay3676 (2020).
3. S. A. Diddams, T. Udem, J. C. Bergquist, E. A. Curtis, R. E. Drullinger, L. Hollberg, W. M. Itano, W. D. Lee, C. W. Oates, K. R. Vogel, and D. J. Wineland, "An optical clock based on a single trapped $^{199}Hg^{+}$ ion," Science **293**, 825–828 (2001).
4. A. D. Ludlow, M. M. Boyd, J. Ye, E. Peik, and P. O. Schmidt, "Optical atomic clocks," Rev. Mod. Phys. **87**, 637–701 (2015).
5. T. Nakamura, I. Ito, and Y. Kobayashi, "Offset-free broadband Yb:fiber optical frequency comb for optical clocks," Opt. Express **23**, 19376–19381 (2015).
6. S. A. Diddams, L. Hollberg, and V. Mbele, "Molecular fingerprinting with the resolved modes of a femtosecond laser frequency comb," Nature **445**, 627–630 (2007).
7. J. D. Gaynor, T. L. Courtney, M. Balasubramanian, and M. Khalil, "Fourier transform two-dimensional electronic-vibrational spectroscopy using an octave-spanning mid-IR probe," Opt. Lett. **41**, 2895–2898 (2016).
8. N. Picqué and T. W. Hänsch, "Frequency comb spectroscopy," Nat. Photonics **13**, 146–157 (2019).
9. K. Minoshima, K. Arai, and H. Inaba, "High-accuracy self-correction of refractive index of air using two-color interferometry of optical frequency combs," Opt. Express **19**, 26095–26105 (2011).
10. I. Coddington, W. C. Swann, L. Nenadovic, and N. R. Newbury, "Rapid and precise absolute distance measurements at long range," Nat. Photonics **3**, 351–356 (2009).
11. V. Torres-Company, J. Schroder, A. Fulop, M. Mazur, L. Lundberg, O. B. Helgason, M. Karlsson, and P. A. Andrekson, "Laser frequency combs for coherent optical communications," J. Lightwave Technol. **37**, 1663–1670 (2019).
12. L. Lundberg, M. Mazur, A. Mirani, B. Foo, J. Schroder, V. Torres-Company, M. Karlsson, and P. A. Andrekson, "Phase-coherent lightwave communications with frequency combs," Nat. Commun. **11**, 201 (2020).
13. S. T. Cundiff and A. M. Weiner, "Optical arbitrary waveform generation," Nat. Photonics **4**, 760–766 (2010).
14. M. Tan, X. Xu, A. Boes, B. Corcoran, J. Wu, T. G. Nguyen, S. T. Chu, B. E. Little, R. Morandotti, A. Mitchell, and D. J. Moss, "Photonic RF arbitrary waveform generator based on a soliton crystal micro-comb source," J. Lightwave Technol. **38**, 6221–6226 (2020).
15. F. Z. Zhang, J. Wu, Y. Li, and J. T. Lin, "Flat optical frequency comb generation and its application for optical waveform generation," Opt. Commun. **290**, 37–42 (2013).
16. E. Obrzud, M. Rainer, A. Harutyunyan, B. Chazelas, M. Cecconi, A. Ghedina, E. Molinari, S. Kundermann, S. Lecomte, F. Pepe, F. Wildi, F. Bouchy, and T. Herr, "Broadband near-infrared astronomical spectrometer calibration and on-sky validation with an electro-optic laser frequency comb," Opt. Express **26**, 34830–34841 (2018).
17. K. P. Nagarjun, V. Jeyaselvan, S. K. Selvaraja, and V. R. Supradeepa, "Generation of tunable, high repetition rate optical frequency combs using on-chip silicon modulators," Opt. Express **26**, 10744–10753 (2018).
18. Z. Z. Lu, H. J. Chen, W. Q. Wang, L. Yao, Y. Wang, Y. Yu, B. E. Little, S. T. Chu, Q. H. Gong, W. Zhao, X. Yi, Y. F. Xiao, and W. F. Zhang, "Synthesized soliton crystals," Nat. Commun. **12**, 3179 (2021).
19. J. N. Kemal, J. Pfeifle, P. Marin-Palomo, M. D. Pascual, S. Wolf, F. Smyth, W. Freude, and C. Koos, "Multi-wavelength coherent transmission using an optical frequency comb as a local oscillator," Opt. Express **24**, 25432–25445 (2016).
20. E. Lucas, P. Brochard, R. Bouchand, S. Schilt, T. Sudmeyer, and T. J. Kippenberg, "Ultralow-noise photonic microwave synthesis using a soliton microcomb-based transfer oscillator," Nat. Commun. **11**, 374 (2020).
21. D. E. Spence, P. N. Kean, and W. Sibbett, "60-fsec pulse generation from a self-mode-locked Ti-sapphire laser," Opt. Lett. **16**, 42–44 (1991).
22. E. Sorokin, S. Naumov, and I. T. Sorokina, "Ultrabroadband infrared solid-state lasers," IEEE J. Sel. Top. Quantum Electron. **11**, 690–712 (2005).
23. Y. M. Chang, H. Kim, J. H. Lee, and Y.-W. Song, "Multilayered graphene efficiently formed by mechanical exfoliation for nonlinear saturable absorbers in fiber mode-locked lasers," Appl. Phys. Lett. **97**, 211102 (2010).
24. A. Bartels, D. Heinecke, and S. A. Diddams, "10-GHz self-referenced optical frequency comb," Science **326**, 681 (2009).
25. T. J. Kippenberg, A. L. Gaeta, M. Lipson, and M. L. Gorodetsky, "Dissipative Kerr solitons in optical microresonators," Science **361**, eaan8083 (2018).
26. V. Brasch, E. Lucas, J. D. Jost, M. Geiselmann, and T. J. Kippenberg, "Self-referenced photonic chip soliton Kerr frequency comb," Light Sci. Appl. **6**, e16202 (2017).
27. H. Weng, J. Liu, A. A. Afridi, J. Li, J. Dai, X. Ma, Y. Zhang, Q. Lu, J. F. Donegan, and W. Guo, "Directly accessing octave-spanning dissipative Kerr soliton frequency combs in an AlN microresonator," Photon. Res. **9**, 1351–1357 (2021).
28. M. Zhang, B. Buscaino, C. Wang, A. Shams-Ansari, C. Reimer, R. Zhu, J. M. Kahn, and M. Loncar, "Broadband electro-optic frequency comb generation in a lithium niobate microring resonator," Nature **568**, 373–377 (2019).
29. A. Parriaux, K. Hammani, and G. Millot, "Electro-optic frequency combs," Adv. Opt. Photon. **12**, 223–287 (2020).
30. M. Song, S. P. Han, J. Park, H. Choi, S. Kim, T. T. Tran, H. D. Kim, and M. Song, "Flat-top supercontinuum generation via Gaussian pulse shaping," Opt. Express **29**, 12001–12009 (2021).
31. K. P. Nagarjun, B. S. Vikram, R. Prakash, A. Singh, S. K. Selvaraja, and V. R. Supradeepa, "Optical frequency comb based on nonlinear spectral broadening of a phase modulated comb source driven by dual offset locked carriers," Opt. Lett. **45**, 893–896 (2020).
32. Z. He, L. Li, J. Zhang, and J. Yao, "Low jitter microwave pulse train generation based on an optoelectronic oscillator," Opt. Express **29**, 33491–33501 (2021).
33. K. Beha, D. C. Cole, P. Del'Haye, A. Coillet, S. A. Diddams, and S. B. Papp, "Electronic synthesis of light," Optica **4**, 406–411 (2017).
34. D. R. Carlson, D. D. Hickstein, W. Zhang, A. J. Metcalf, F. Quinlan, S. A. Diddams, and S. B. Papp, "Ultrafast electro-optic light with subcycle control," Science **361**, 1358–1362 (2018).
35. A. Cerqueira, J. M. C. Boggio, A. A. Rieznik, H. E. Hernandez-Figueroa, H. L. Fragnito, and J. C. Knight, "Highly efficient generation of broadband cascaded four-wave mixing products," Opt. Express **16**, 2816–2828 (2008).

36. E. Myslivets, B. P. P. Kuo, N. Alic, and S. Radic, "Generation of wide-band frequency combs by continuous-wave seeding of multistage mixers with synthesized dispersion," Opt. Express **20**, 3331–3344 (2012).
37. V. Ataie, E. Myslivets, B. P. P. Kuo, N. Alic, and S. Radic, "Spectrally equalized frequency comb generation in multistage parametric mixer with nonlinear pulse shaping," J. Lightwave Technol. **32**, 840–846 (2014).
38. T. Inoue and S. Namiki, "Pulse compression techniques using highly nonlinear fibers," Laser Photon. Rev. **2**, 83–99 (2008).
39. M. Zajnulina, J. M. C. Boggio, M. Bohm, A. A. Rieznik, T. Fremberg, R. Haynes, and M. M. Roth, "Generation of optical frequency combs via four-wave mixing processes for low- and medium-resolution astronomy," Appl. Phys. B **120**, 171–184 (2015).
40. X. Zhang, J. Zhang, K. Yin, Y. Li, X. Zheng, and T. Jiang, "Sub-100 fs all-fiber broadband electro-optic optical frequency comb at 15 μm," Opt. Express **28**, 34761–34771 (2020).
41. R. G. Smith, "Optical power handling capacity of low loss optical fibers as determined by stimulated Raman and Brillouin-scattering," Appl. Opt. **11**, 2489–2494 (1972).
42. Q. Li, Z. X. Jia, Z. R. Li, Y. D. Yang, J. L. Xiao, S. W. Chen, G. S. Qin, Y. Z. Huang, and W. P. Qin, "Optical frequency combs generated by four-wave mixing in a dual wavelength Brillouin laser cavity," AIP Adv. **7**, 075215 (2017).
43. Y. L. Huang, Q. Li, J. Y. Han, Z. X. Jia, Y. S. Yu, Y. D. Yang, J. L. Xiao, J. L. Wu, D. M. Zhang, Y. Z. Huang, W. P. Qin, and G. S. Qin, "Temporal soliton and optical frequency comb generation in a Brillouin laser cavity," Optica **6**, 1491–1497 (2019).
44. H. Z. Weng, J. Y. Han, Q. Li, Y. D. Yang, J. L. Xiao, G. S. Qin, and Y. Z. Huang, "Optical frequency comb generation based on the dual-mode square microlaser and a nonlinear fiber loop," Appl. Phys. B **124**, 91 (2018).
45. F. Ferdous, H. X. Miao, D. E. Leaird, K. Srinivasan, J. Wang, L. Chen, L. T. Varghese, and A. M. Weiner, "Spectral line-by-line pulse shaping of on-chip microresonator frequency combs," Nat. Photonics **5**, 770–776 (2011).
46. H. Long, Y. Z. Huang, X. W. Ma, Y. D. Yang, J. L. Xiao, L. X. Zou, and B. W. Liu, "Dual-transverse-mode microsquare lasers with tunable wavelength interval," Opt. Lett. **40**, 3548–3551 (2015).
47. H. Long, Y. Z. Huang, Y. D. Yang, L. X. Zou, X. M. Lv, B. W. Liu, J. L. Xiao, and Y. Du, "Mode characteristics of unidirectional emission AlGaInAs/InP square resonator microlasers," IEEE J. Quantum Electron. **50**, 981–989 (2014).
48. J. Y. Han, Y. L. Huang, J. L. Wu, Z. R. Li, Y. D. Yang, J. L. Xiao, D. M. Zhang, G. S. Qin, and Y. Z. Huang, "10-GHz broadband optical frequency comb generation at 1550/1310 nm," Opto-Electron. Adv. **3**, 190033 (2020).
49. M. Erkintalo, Y. Q. Xu, S. G. Murdoch, J. M. Dudley, and G. Genty, "Cascaded phase matching and nonlinear symmetry breaking in fiber frequency combs," Phys. Rev. Lett. **109**, 223904 (2012).
50. J. M. Dudley, G. Genty, and S. Coen, "Supercontinuum generation in photonic crystal fiber," Rev. Mod. Phys. **78**, 1135–1184 (2006).
51. J. M. Dudley and S. Coen, "Fundamental limits to few-cycle pulse generation from compression of supercontinuum spectra generated in photonic crystal fiber," Opt. Express **12**, 2423–2428 (2004).